Research on Chemical Intermediates (2025) 51:1989–2005
https://doi.org/10.1007/s11164-025-05547-y

Opto-electronic studies and diode applications: synthesis, characterization, and photoconductive properties of Schiff base and its Pd(II) and Pt(II) complexes

Nevin Turan[1] · Kenan Buldurun[2] · Halil Seymen[3] · Bayram Gündüz[4] · Naki Çolak[5]

Received: 22 December 2024 / Accepted: 27 February 2025 / Published online: 12 March 2025

Abstract

This research involved the creation of a Schiff base ligand, (*E*)-6-tert-butyl 3-ethyl 2-(3-methoxy-4-phenoxybenzylideneamino)-4,5-dihydrothieno[2,3-*c*]pyridine-3,6(7H)-dicarboxylate (SB), through the condensation reaction of 6-tert-butyl 3-ethyl 2-amino-4,5-dihydrothieno[2,3-*c*]pyridine-3,6(7H)-dicarboxylate with 3-methoxy-4-phenoxybenzaldehyde. The synthesized Schiff base was then used to form metal complexes with Pd(II) and Pt(II) metal ions. Various analytical techniques, including microanalysis (C, H, N, and S), FT-IR, ^{1}H-NMR, ^{13}C-NMR, UV–Vis., thermal analysis (TGA), powder XRD analysis, mass (ESI), molar conductivity, and magnetic susceptibility, were employed to confirm the structures of synthesized compounds. Spectroscopic data indicated that the Schiff base functions as a chelating agent, utilizing oxygen and nitrogen donor sites. The molar conductance measurements suggested that both complexes are non-electrolytic. A square planar structure was proposed for the Pd(II) and Pt(II) complexes. The study also investigated the electronic and photonic characteristics of the metal complexes under different conditions. Furthermore, a basic diode was fabricated using the metal complex, and its electronic and photonic characteristics were thoroughly investigated. Current–voltage (I-V) measurements showed that the diode based on the Pd(II) complex had notable noise and a high leakage current. On the other hand, the diode with the Pt(II) complex exhibited enhanced photoconductivity as the light intensity increased.

Extended author information available on the last page of the article

Graphical abstract

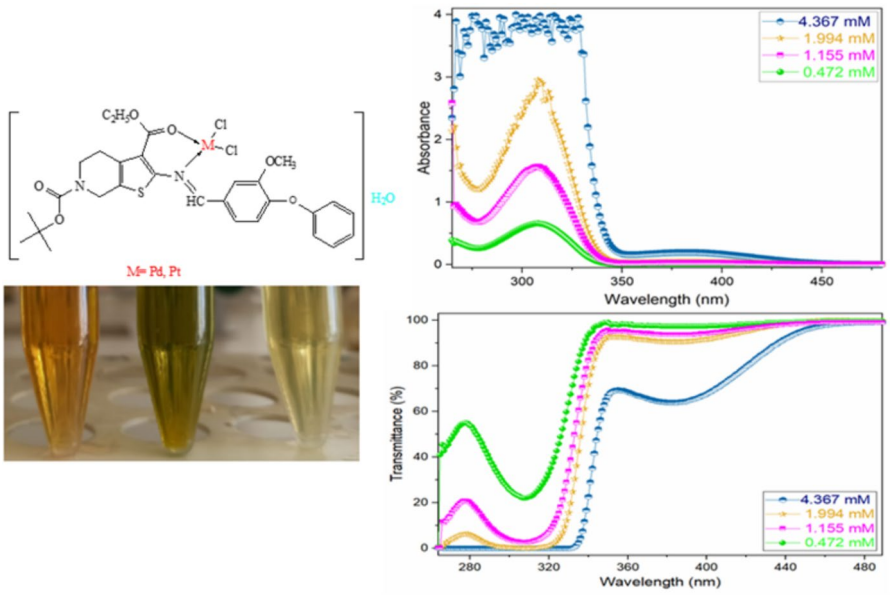

Keywords Photoconductive · Opto-electronic · Diode · Schiff base · Pt(II) and Pd(II) complexes · Spectroscopic methods

Introduction

Schiff bases are organic compounds formed when the carbonyl group of aldehydes or ketones reacts to produce an azomethine or imine group, with or without a catalyst, under certain conditions. These reactions are reversible and typically take place most effectively in mildly acidic environments [1]. The study of Schiff bases and their metal complexes has seen growing interest, leading to increased synthesis of novel compounds with varied properties and applications. While initial research concentrated on compound creation, recent efforts have expanded into broader application domains [2]. Metal complexes of Schiff bases are notable for their roles in catalysis [3–5], analytical applications [6], oxygen reabsorption in epoxidation reactions [7], photochromic characteristics, fluorescence properties [7, 8], and their ability to form complexes with certain toxic metals [9]. In living systems and pharmaceutical chemistry, transition metal ions are crucial due to their chemical properties that enable complex formation with appropriate ligands. The pharmacological activities of these complexes are influenced by the metal ions, ligands, and complex structure [10–13], which determine their ability to reach specific target sites in the body. Moreover, metal carbonyl derivatives are significant in various homogeneous catalytic processes, including hydrogenation, hydroformylation, carbonylation, and oxygen transfer reactions [14–16]. Coordination

complexes involving nitrogen and sulfur donor ligands have been extensively studied, often revealing unique structural characteristics. The use of Schiff base compounds as analytical reagents is growing, particularly for the detection of various inorganic and organic substances [1, 17].

A current technological advancement involves research on semiconductor usage processes. Semiconductors are materials whose conductivity can be adjusted based on doping type and quantity. These easily processed materials, which are relatively cost-effective compared to metals, have garnered researcher interest [17, 18]. Structures known as Schottky diodes, based on Walter H. Schottky's work, form the foundation of metal–semiconductor (MS) material studies [19]. These structures serve as rectifiers. Many physics and chemistry researchers are working to develop new materials for semiconductor technology, including research on diodes with novel properties using both inorganic and organic materials [20]. Recently, ligands fundamental to metal complexes, have gained attention in optoelectronic device research. Studies indicate that Schiff bases and metal complexes can be utilized in photodiode, transistor, and photovoltaic applications in conjunction with organic materials [21–23].

This work aims to demonstrate the synthesis and structural analysis of the newly synthesized Schiff base and its Pd(II) and Pt(II) complexes and to investigate their electronic and photonic properties. Additionally, the research includes the fabrication of basic diodes using the metal complex.

Materials and method

The compounds were synthesized using commercially acquired reagents and solvents from Sigma & Aldrich, which were utilized without further purification. Elemental analysis (C, H, N, and S) was performed using a Leco CHNS-O model 932 analyzer. A Shimadzu UV-1800 spectrophotometer was employed to obtain electronic spectra in DMF ($\approx 10^{-5}$ mol^{-1}). ^{1}HNMR and ^{13}C NMR spectra were recorded on a Bruker 400 Mercury spectrometer, with $CDCl_3$ and DMSO-d_6 as the solvent and Me_4Si as the internal standard. FT-IR spectra were collected in the 4000–400 cm^{-1} range using a Perkin Elmer-65 spectrophotometer with KBr pellets. Mass spectra were obtained on an AGILENT model 1100 MSD mass spectrometer utilizing electron spray ionization. Magnetic measurements were conducted on a Sherwood Auto Magnetic Susceptibility Balance using the Gouy method, with $Hg[Co(NCS)_4]$ as the calibrator. Molar conductance of the complexes in DMF (10^{-3} M) solutions was measured using a Jenway 4010 conductivity meter. Thermogravimetric analyses (TGA) were performed on a Shimadzu DTG-60 AH with a heating rate of 10 °C/min under a nitrogen atmosphere. Powder XRD patterns were acquired using a Bruker D8 Advance diffractometer with Cu Kα radiation ($\lambda = 1.5406$ Å).

Synthesis of Schiff base ligand

In a round-bottom flask containing 20 mL of ethanol, 6-tert-butyl 3-ethyl 2-amino-4,5-dihydrothieno[2,3-*c*]pyridine-3,6(7H)-dicarboxylate (0.60 g, 1.83 mmol) was

placed. Subsequently, 3-methoxy-4-phenoxybenzaldehyde (0.42 g, 1.83 mmol) was introduced into the same flask at ambient temperature, with continuous agitation for 30 min. The resulting mixture underwent reflux for 3 h. Upon cooling, the reaction solution was adjusted to a pH between 3 and 4 using glacial acetic acid. The progress of the reaction was checked by TLC using a solvent system of n-hexane and ethyl acetate (1:1) ratio. The mixture then underwent recrystallization from ethanol, and the resulting yellow solid was isolated through filtration and rinsed with ethanol. The preparation of the starting material followed the method described in the literature [24]. Figure 1 illustrates the synthetic pathway for the Schiff base ligand.

Yield 82%. m.p. 151–153 °C. Anal. calcd for $C_{29}H_{32}N_2O_6S$ (FW: 536.64 g/mol) (%): C, 64.90; H, 5.96; N, 5.21; S, 5.96; Found (%): C, 65.00; H, 5.98; N, 5.20; S, 5.99. FT-IR (KBr pellet, ν, cm^{-1}): 3149, 3058 $(-CH)_{Ar}$, 2975, 2933 $(-CH)_{Alip}$, 1677, 1660 (C=O), 1583 (CH=N), 1550, 1486, 1475, 1425 $(C=C)_{Ar}$, 1266 (-OC), 1168 $(-OCH_3)$, 779 (C-S-C). ^{1}H-NMR (δ, ppm, chloroform-d): 8.26 (H, s, CH=N), 7.29–7.27 (H, dd, J=7.28 Hz, $CH)_{Ar}$, 7.25–7.23 (H, dd, J=7.24 Hz, $CH)_{Ar}$, 7.22 (H, s, $CH)_{Ar}$, 7.21, 7.20 (H, d, J=7.21 Hz, $CH)_{Ar}$, 7.01–6.99 (2H, dd, J=7.00 Hz, $CH)_{Ar}$, 6.99–6.97 (H, d, J=6.98 Hz, $CH)_{Ar}$, 6.96–6.93 (H, d, J=6.94 Hz, $CH)_{Ar}$, 4.72 (2H, s, $CH_2)_{py}$, 4.35–4.32 (2H, q, J=4.33 Hz, OCH_2CH_3), 3.57–3.53 (2H, t, J=3.55 Hz, $CH_2)_{py}$, 2.91–2.89 (2H, t, J=2.90 Hz, $CH_2)_{py}$, 3.53 (3H, s, OCH_3), 1.50 (9H, s, $-CH_3$), 1.40–1.38 (3H, t, J=1.39 Hz, $-OCH_2CH_3$). ^{13}C-NMR (δ, ppm, chloroform-d): 157.45, 156.66 (2C=O), 158.36 (CH=N), 154.50, 151.99, 151.03, 146.55, 136.03, 130.06, 125.73, 124.53, 123.49, 119.24, 117.36, 112.69, 111.48, 43.40, 23.55 (Ar. -C), 80.96, 61.50, 56.78, 28.41, 14.69 (Alip. -C). UV–Vis. (λ_{max}, nm): 215, 246, 270, 296 ($\pi \rightarrow \pi^*$); 312, 350, 378 ($n \rightarrow \pi^*$). ES-MS: m/z 537.64 (Calcd), 537.18 (Found) $[M+H]^+$.

Synthesis of Schiff base metal complexes

In a two-necked 250 mL ground-glass flask, 0.40 g (1.10 mmol) of SB ligand was measured and introduced. The ligand was then dissolved in toluene with the aid of heat. A solution containing 0.70 g (1.10 mmol) of $PdCl_2(CH_3CN)_2$ in toluene was subsequently added, resulting in a noticeable color change. The mixture was then refluxed under inert conditions at 95 °C for 7 h. Following this, the resulting precipitate was isolated through suction filtration and purified by multiple washes using petroleum ether and toluene. The product was then dried in vacuum desiccators. Figure 2 shows the proposed structure of the synthesized Pd(II) complex.

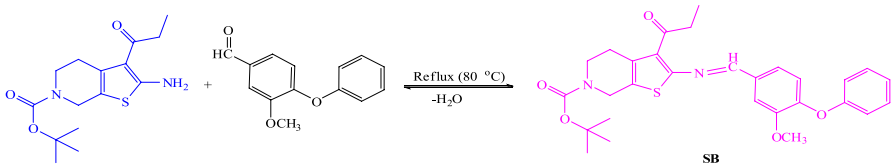

Fig. 1 Synthesis of SB. *(E)−6-tert-butyl 3-ethyl 2-(3-methoxy-4-phenoxybenzylideneamino)−4,5-dihydrothieno[2,3-c]pyridine-3,6(7H)-dicarboxylate (SB)*

[$SBPdCl_2$]•H_2O: Brown solid, yield 75%. m.p. 221–223 °C. Anal. calcd for $C_{29}H_{34}N_2O_7SPdCl_2$ (FW: 731.67 g/mol) (%): C, 47.60; H, 4.64; N, 3.82; S, 4.38; Found: C, 47.64; H, 4.68; N, 3.86; S, 4.41. FT-IR (KBr pellet, ν cm^{-1}): 3419 (OH/H_2O), 3157 (-CH)$_{Ar}$, 2979, 2933 (-CH)$_{Alip}$, 1693, 1677 (C=O), 1589 (CH=N), 1566, 1535, 1467 (C=C)$_{Ar}$, 1236 (-OC), 1168 (-OCH_3), 781 (C-S-C), 597, 523 (M–O), 468 (M–O). ^{1}H-NMR (δ, ppm, dmso-d_6): 8.34 (H, s, CH=N), 7.39–7.37 (H, dd, J=7.38 Hz, CH)$_{Ar}$, 7.31–7.29 (H, dd, J=7.30 Hz, CH)$_{Ar}$, 7.26 (H, s, CH)$_{Ar}$, 7.01–7.03 (2H, dd, J=7.02 Hz, CH)$_{Ar}$, 6.94–6.90 (H, d, J=6.92 Hz, CH)$_{Ar}$, 4.56 (2H s, $CH_2)_{py}$, 4.41–4.39 (2H, q, J=4.40 Hz, OCH_2CH_3), 3.72 (2H, s, J=3.65 Hz, $CH_2)_{py}$, 3.60 (3H, s, OCH3), 2.96–2.82 (4H, t, J=2.88 Hz, $CH_2)_{py}$, 1.50 (9H, s, -CH_3), 1.42–1.40 (3H, t, J=1.41 Hz, -OCH_2CH_3). ^{13}C-NMR (δ, ppm, dmso-d_6): 166.55, 163.68 (C=O), 165.25 (CH=N), 143.87, 140.22, 139.72, 135.85, 129.42, 123.28, 118.64, 114.77, 108.33, 42.40, 41.60, 23.21 (Ar. -C), 79.73, 56.48, 39.34, 28.51, 14.87 (Alip. -C). UV–Vis. (λ_{max}, nm): 226, 257, 283, 292 ($\pi \rightarrow \pi^*$); 309, 321, 397 ($n \rightarrow \pi^*$); 459, 729 (d-d, LMCT). ES-MS: *m/z* 732.67 (Calcd), 732.30 (Found) $[M+H]^+$. μ_{eff} (B.M.): Dia. Molar conduc. (10^{-3} M, DMF): 18.50 Ω^{-1} cm^2 mol^{-1}.

In a two-necked 250 mL ground flask, SB ligand (0.40 g, 1.10 mmol) was dissolved in methanol (20 mL). A mixture of K_2PtCl_4 (0.46 g, 1.10 mmol) in methanol (15 mL) and deionized water (10 mL) was subsequently added to the flask. The reaction proceeded under reflux conditions in an inert atmosphere for 48 h. Following this period, a portion of the solvent was removed from the reaction mixture using low pressure and appropriate conditions. The resulting product, with all solvent removed, underwent washing with pure water and methanol. It was then crystallized using a dichloromethane/diethyl ether mixture and air-dried. The proposed structure of the Pt(II) complex is depicted in Fig. 2.

[$SBPtCl_2$]•H_2O: Dark brown solid, yield: 73%. m.p. > 300 °C. Anal. calcd for $C_{29}H_{34}N_2O_7SPtCl_2$ (FW: 820.33 g/mol) (%): C, 42.46; H, 4.14; N, 3.41; S, 3.90; Found: C, 42.50; H, 4.12; N, 3.44; S, 3.92. IR (KBr pellet, ν cm^{-1}): 3430 (OH/H_2O), 3070 (-CH)$_{Ar}$, 2925, 2850 (-CH)$_{Alip}$, 1677, 1651 (C=O), 1609 (CH=N), 1558, 1509, 1497, 1406 (-C=C)$_{Ar,}$ 1242 (-OC), 1169 (-OCH_3), 782 (C-S-C), 595, 527 (M–N), 499, 455 (M–O). ^{1}H-NMR (δ, ppm, dmso-d_6): 8.43 (H, s, CH=N), 7.22 (H, dd, J=7.22 Hz, CH)$_{Ar}$, 7.20 (H, s, CH)$_{Ar}$, 7.18 (H, dd, J=7.18 Hz, CH)$_{Ar}$, 716 (H, d, J=7.16 Hz, CH)$_{Ar}$, 6.99–6.97 (H, dd, J=6.98 Hz, CH)$_{Ar}$, 6.98–6.96 (H, d, J=6.97 Hz, CH)$_{Ar}$, 6.95 (H, d, J=6.95 Hz, CH)$_{Ar}$, 6.93 (H, d, J=6.93 Hz, CH)$_{Ar}$, 4.43 (2H, s, $CH_2)_{py}$, 4.36–4.27 (2H, q, J=4.33 Hz, OCH_2CH_3), 3.33–3.32 (2H, t,

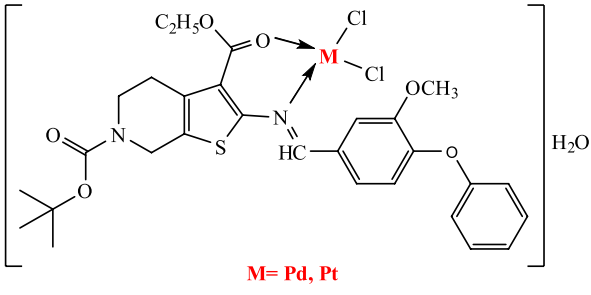

Fig. 2 Proposed structures of metal complexes

$J = 3.33$ Hz, $CH_2)_{py}$, 2.91–2.88 (2H, t, $J = 2.89$ Hz, $CH_2)_{py}$, 3.83 (3H, s, OCH_3), 1.50 (9H, s, $-CH_3$), 1.38–1.35 (3H, t, $J = 1.37$ Hz, $-OCH_2CH_3$). ^{13}C-NMR (δ, ppm, dmso-d_6): 158.35, 156.66 (2C=O), 157.45 (CH=N), 152.32, 151.99, 146.55, 135.05, 125.73, 124.53, 123.49, 119.24, 117.36, 112.69, 111.48, 43.54, 43.40, 23.55 (Ar. -C), 80.96, 61.50, 56.78, 28.41, 14.69 (Alip. -C). U V–Vis (λ_{max}, nm): 229, 252, 285, 297 ($\pi \rightarrow \pi^*$); 314, 337 ($n \rightarrow \pi^*$), 496, 661, 751 (d-d, LMCT). ES-MS: *m/z* 822.33 (Calcd), 822.16 (Found) $[M+2H]^+$. μ_{eff} (B.M.): Dia. Molar conduc. (10^{-3} M, DMF): 15.10 Ω^{-1} cm^2 mol^{-1}.

The powder X-ray diffraction analysis

X-ray diffraction analyses were conducted on the Pd(II) and Pt(II) complexes, covering a range of 5–90° at a wavelength of 0.1540562 nm. The resulting diffractograms and their accompanying data provide information on each peak's 2Θ value, relative intensity, and the spacing between atomic planes.

Results and discussion

NMR spectra

In the ^{1}H-NMR spectra, the SB ligand's azomethine (CH=N) proton was observed as a single peak at 8.26 ppm. After coordination to Pt(II) and Pd(II), the azomethine peak shifted downfield to 8.34 and 8.35 ppm due to the interaction of azomethine groups with Pt(II) and Pd(II) ions [25, 26]. The ^{13}C{H}NMR spectra of SB revealed signals for carbonyl and azomethine group carbons at 165.26, 153.38, and 163.99 ppm. Both complexes exhibited higher ppm shifts for the characteristic azomethine proton and carbon, carbonyl carbon signals compared to the free ligand, confirming the complexes' binding to azomethine nitrogen and carbonyl oxygen. The shift in these carbon atoms' peaks during complex formation further validates the occurrence of coordination. The ^{1}H and ^{13}C-NMR spectra of the SB and its Pt(II) and Pd(II) complexes were obtained using $CDCl_3$ and DMSO-d_6 as the solvent, and the spectra are presented in Figs. S1–S6 (Supplementary info).

IR spectra

The infrared (IR) spectrum of the SB ligand exhibited characteristic bands at approximately 1677 and 1660, 1583, 1266, 1168, and 779 cm^{-1}, which were attributed to the stretching vibrations of C=O, CH=N, -OC, OCH_3, and C-S-C, respectively. The IR spectra for both the SB and its palladium(II) and platinum(II) complexes are available in the supplementary materials (Figs. S7–S9). Bands at 1693, 1677 and 1677, 1651 cm^{-1} were attributed to the carbonyl group's stretching vibration, while those at 1589 and 1609 cm^{-1} were associated with the CH=N group's stretching vibration. These shifts indicate that the SB coordinates through the azomethine groups' N atom and the carbonyl groups' O atom, functioning as a bidentate

ligand. Furthermore, new intensity bands appeared in the ranges of 597–523 and 499–455 cm^{-1} in the metal complexes, suggesting the formation of M–N and M–O stretching vibrations [27]. The C-S-C characteristic band in the SB remained largely unchanged in the metal complexes' IR spectra, indicating that C-S-C does not coordinate with the metal center. The complexes' IR spectra showed broad bands at 3430 and 3419 cm^{-1}, attributable to the OH stretching of hydration water molecules attached to the metal complexes [28]. This observation was corroborated by elemental and thermal analysis results [29]. All expected aromatic ring characteristic bands were also observed in the metal complexes.

UV–vis spectra and magnetic moment measurements

The SB ligand's electronic spectra displayed absorption peaks between 296 and215 nm and 378–312 nm, corresponding to $\pi \rightarrow \pi^*$ and $n \rightarrow \pi^*$ transitions, respectively [30, 31]. For the complexes, UV–Vis spectra showed peaks in the 292–226 nm range, likely due to $\pi \rightarrow \pi^*$ transitions, while peaks between 337 and 309 nm were attributed to $n \rightarrow \pi^*$ transitions from carbonyl chromophores and azomethine groups. The Pd(II) complex exhibited bands at 397, 459, and 729 nm, assigned to $^1A_{1g} \rightarrow {}^1E_g$, $^1A_{1g} \rightarrow {}^1B_g$, and $^1A_{2g} \rightarrow {}^1A_{1g}$ transitions, indicating square planar geometry [32]. The Pt(II) complex, being diamagnetic with a low-spin d^8 system, showed spin-allowed d-d transition at 496 nm ($^1A_{2g} \rightarrow {}^1A_{1g}$), confirming square planar geometry. Unlike the ligand, both complexes showed transitions at 496 and 459 nm due to ligand-to-metal charge transfer. The Pt(II) complex spectrum displayed less intense, broad bands at 661, 751, and 982 nm, primarily from overlapping azomethine and carbonyl group $\pi \rightarrow \pi^*$ energy transitions and LMCT transitions involving carbonyl O and platinum-bound azomethine N donor lone pairs [31, 33]. The effective magnetic moment values at room temperature (28 °C) indicated diamagnetic properties for both complexes.

Molar conductance and mass spectrum

Molar conductance measurements in DMF yielded values of 18.50 for Pd(II) and 15.10 Ω^{-1} cm^2 mol^{-1} for Pt(II) [34, 35], suggesting non-electrolytic nature. Mass spectra confirmed the molecular mass of Pd(II) and Pt(II) complexes, with experimental ion peaks at m/z 732.67 and 822.33 corresponding to $[M+H]^+$ and $[M+2H]^+$ molecular ions, respectively. These values aligned well with theoretical calculations. The presence of molecular ion peaks in the mass spectra suggests that the complex is non-electrolytic, with two bidentate ligands bound through O and N donor atoms, resulting in quadruple coordination [36].

The thermal analysis

The synthesized complexes' thermal characteristics were investigated from 25 to 900 °C under nitrogen, with a 20 °C min^{-1} heating rate. Decomposition of the palladium and platinum complexes occurred in 3 and 2 phases, respectively. The first

phase, between 50 and 170 °C, showed the loss of lattice water molecules from both complexes' coordination spheres [37, 38]. The second phase, from 170 to 500 °C, involved the organic SB moiety's elimination. The groups separated in subsequent phases and their corresponding mass losses in the synthesized complex compounds are shown in Table 1. Thermogram analysis indicated that decomposition continued above 500 °C. Figs. S16 and S17 (Supplementary info) display the thermal analysis spectra for the Pd(II) and Pt(II) complexes.

Various analytical and spectroscopic techniques were employed to confirm the structures of the synthesized complexes. The complexes' 1:1 metal: ligand ratio was established through elemental analysis, stoichiometric data, and spectroscopic findings. A square planar structure is exhibited by all the complexes.

The powder XRD studies

The Pd(II) and Pt(II) complexes could not be obtained as single crystals. To evaluate their crystalline structure, XRD analysis was conducted. The diffraction measurements were performed using a Rigaku Ultima IV X-ray diffractometer with CuKα radiation (λ = 0.1540562 nm). XRD analysis parameters included a 0.02° scan step size, 5° to 90° scanning range, 2Theta/Theta scanning mode, continuous scanning type, and an operating current and voltage of 40 mA and 40 kV, respectively. Figure 3 displays the resulting diffraction patterns for both Pd(II) and Pt(II) complexes. Scherer's equation was employed to estimate the grain sizes of the complexes.

$$D = \frac{z\lambda}{F.Cos\theta} \tag{1}$$

In this equation, λ represents the wavelength of X-rays, θ denotes the angle of Bragg diffraction, and z is a constant equal to 1.54 for cubic symmetry spherical crystals. F signifies the full width at half maximum (FWHM) of the diffraction peak. The highest peak intensity was used to determine the average grain size (D) for each complex. A summary of the estimated crystal parameters for the complexes is provided in Table 2. This includes FWHM, grain size, diffraction angles, peak intensity, and relative intensity (expressed as a percentage of the highest peak). Only

Table 1 Thermal analytical data for Pd(II) and Pt(II) complexes

Complexes	Step	Temperature (°C)	TG mass loss (%) Calculated/Found		Separated groups
$[SBPdCl_2]•H_2O$	1	50–170	2.46	2.86	H_2O
	2	170–290	26.63	25.69	Cl_2, $C_7H_8O_2$
	3	290–500	19.95	20.14	$C_7H_{14}O_3$
	Residue			51%	
$[SBPtCl_2]•H_2O$	1	50–120	2.19	1.70	H_2O
	2	120–500	53.99	53.17	Cl_2, $C_{21}H_{26}O_5N$
	Residue			45%	

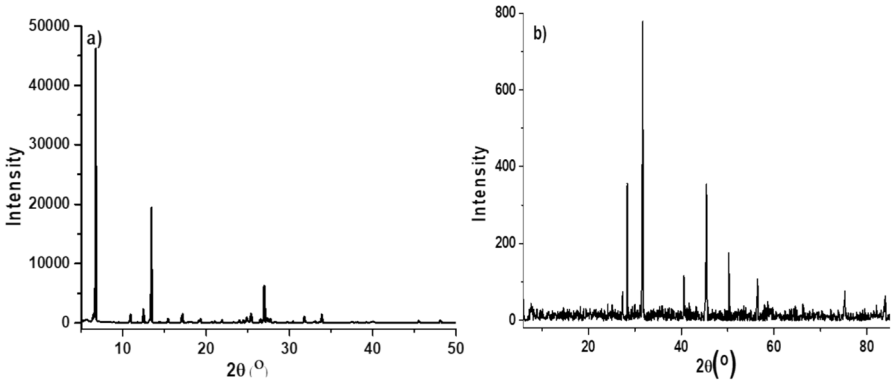

Fig. 3 Powder XRD pattern of Pd(II) and Pt(II) complexes

peaks with an intensity of at least 5% of the maximum peak were considered in the analysis.

XRD results of Pd(II) complex

Figure 3a illustrates the XRD analysis of the Pd(II) complex, which exhibited multiple distinctive peaks of varying intensities. The most significant peak was detected at 6.74°, while the weakest peak was observed at 23.28°. A comparison of these XRD powder peaks with the MDI JADE library indicated a close match to the

Table 2 The predicted powder XRD parameters of the Pd(II) and Pt(II) complexes

2 Theta(°)	FWHM(°)	Intensity	Relative intensity %	D nm	Average
6.741	0.061	46,029	100	130.4599	102.0677
12.472	0.094	2324	5	85.01676	
13.431	0.072	19,502	42.4	111.0996	
26.966	0.101	6293	13.7	80.8856	
					2
27.41	0.118	58	7.5	69.29749	55.95408
28.428	0.099	342	44.3	82.77961	
31.763	0.153	773	100	53.98404	
40.659	0.158	108	13.9	53.62031	
45.492	0.195	352	45.5	44.17557	
50.343	0.091	171	22.1	96.45983	
56.538	0.204	105	13.6	44.21608	
66.284	0.241	39	5.1	39.36837	
75.339	0.268	75	9.7	37.44919	
84.038	0.28	60	7.8	38.19032	

monoclinic crystal structure of dicloxacillin ($C_{19}H_{16}Cl_2N_3NaO_5S$, PDF#32–1648). As shown in Table 2, the average grain size of the Pd(II) complex was determined to be 102.07 nm. The largest grain size, measuring 130.46 nm, corresponded to a diffraction angle of 6.74°, whereas the smallest grain size of 80.88 nm was associated with a diffraction angle of 26.97°.

XRD analysis of Pt(II) complex

Figure 3b illustrates the XRD phase behavior of the Pt(II) complex. Multiple peaks were identified with intensities surpassing the background noise. The most prominent peak was detected at 31.76°, while the least intense peak appeared at 66.28°. A comparison of these XRD peaks with the MDI JADE database revealed a close match to the Monoclinic crystal structure of cis-platinum ammine chloride dimethyl sulfoxide $C_2H_9Cl_2NOPtS$ (PDF#38–1959). The Pt(II) complex exhibited an average grain size of 55.95 nm, with all related measurements presented in Table 2. The largest grain size, measuring 96.46 nm, was observed at a diffraction angle of 50.34°, whereas the smallest grain size of 37.45 nm was found at a diffraction angle of 75.34°.

Electronics and photonics studies

The absorbance patterns of the Pt(II) metal complex at various concentrations (4.367, 1.994, 1.155, and 0.472 mM) are illustrated in Fig. 4 as a function of wavelength. The graph demonstrates that the absorbance values of the Pt(II) metal complex increase proportionally with concentration. Additionally, the complex consistently shows a peak absorption at approximately 310 nm wavelength.

The transmittance curves of the Pt(II) complex at various concentrations are shown in Fig. 5a. The data reveals that as the concentration increases, the transmittance of the Pt(II) metal complex decreases. Moreover, at higher wavelengths, the transmittance values exhibit a rapid increase within specific ranges before reaching and stabilizing at their maximum levels.

Figure 5b displays the 1st derivatives of the transmittance values plotted against wavelength, from which the absorption band edge values of the Pt(II) metal complex were determined for concentrations of 4.367, 1.994, 1.155, and 0.472 mM. These values are presented in Table 3. The data in Table 3 demonstrates an inverse relationship between the concentration of the Pt(II) metal complex and its absorption band edge value, with higher concentrations corresponding to lower absorption band edge values.

The optical band gap (Eg) values of Pt(II) metal complex at concentrations of 4.367, 1.994, 1.155 and 0.472 mM were obtained by using Eq. (2).

$$\alpha = \frac{B(h\upsilon - E_g)^m}{h\vartheta} \tag{2}$$

In this equation, B represents the constant, hυ denotes the energy of a photon, and Eg signifies the optical band gap of the material. Figure 6 illustrates the

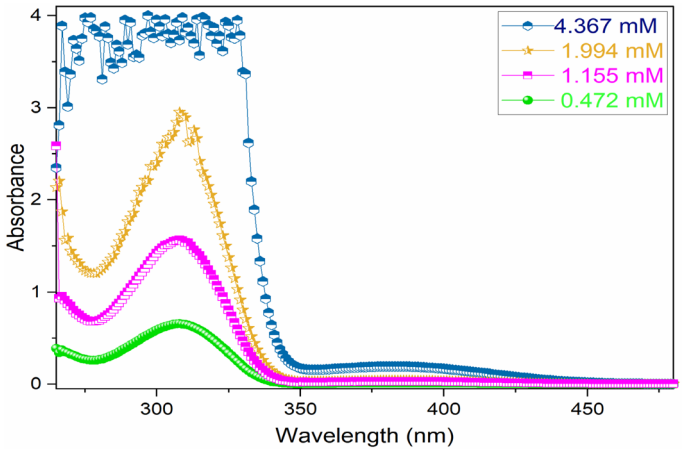

Fig. 4 Absorbance curves versus wavelength of Pt(II) metal complex at concentrations of 4.367, 1.994, 1.155, and 0.472 mM

plot of E versus $(\alpha h\upsilon)^2$, which is used to determine the Eg values of the Pt(II) metal complex at concentrations of 4.367, 1.994, 1.155, and 0.472 mM. A linear region is observed, and the optical band gap values for the Pt(II) metal complex at these concentrations were calculated to be 3.483, 3.598, 3.626, and 3.672 eV, respectively. It is noted that the optical band value of the Pt(II) metal complex exhibits an inverse relationship with concentration, decreasing as the concentration increases.

The refractive index values of the Pt(II) metal complex at the specified concentrations were calculated using various methods (Ravindra, Moss, Kumar, Reddy, Singh and Herve-Van Damme), with the results shown in Table 3. The analysis reveals that the Ravindra relation yields the smallest values, whereas the Reddy relation produces the largest.

Preparation of Pt(II) metal complex based diode

This research involved the fabrication of diodes using identical methods for Pd(II) and Pt(II) metal complexes, followed by current–voltage (I-V) measurements. The I-V measurements for the Pd(II) complex were found to be insignificant, likely due to its unsuitable properties for diode production, including forbidden energy ranges, absorption characteristics, and leakage currents. Consequently, this discussion focuses on the preparation, measurements, and results of the Pt(II) metal complex-based diode.

The Pt(II) metal complex-based diode was constructed using p-type silicon. The Si layer's oxide coating was eliminated using HF/H_2O solution, followed by rinsing in deionized water in an ultrasonic bath for chemical cleaning. The prepared p-Si was placed in a vacuum system, and Ag metal was evaporated onto its back surface to create an ohmic contact. A Pt(II) metal complex solution was then prepared and

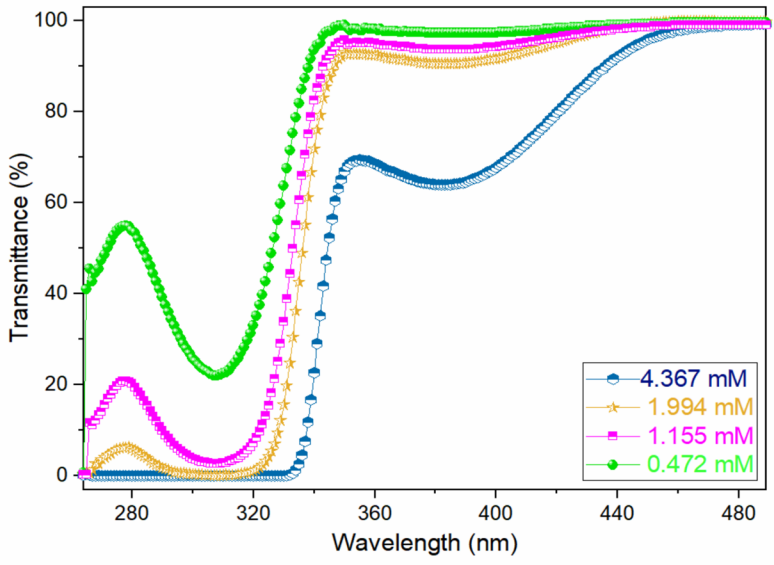

a)

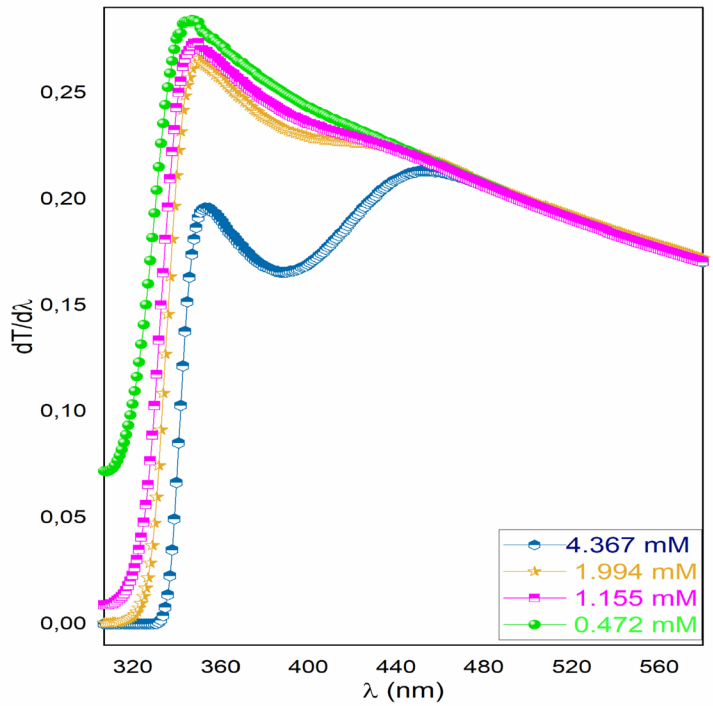

b)

Fig. 5 The **a** transmittance and **b** dT/dλ spectra as a function of wavelength for the Pt(II) complex at concentrations of 2.609, 0.520, and 0.238 mM

Table 3 The absorption band edge (EAbs-edge) and refractive index values for the Pt(II) complex at concentrations of 2.609, 0.520, and 0.238 mM were calculated using various relations

Molarity (mM)	$E_{Abs\text{-}edge}$ (eV)	Refractive index values					
		Moss	Ravindra	Herve-Vandamme	Reddy	Kumar–Singh	Average
4.367	3.513	2.285	1.925	2.197	2.651	2.252	2.262
1.994	3.543	2.267	1.853	2.169	2.627	2.228	2.229
1.155	3.573	2.262	1.836	2.162	2.621	2.223	2.221
0.472	3.543	2.255	1.807	2.151	2.612	2.214	2.208

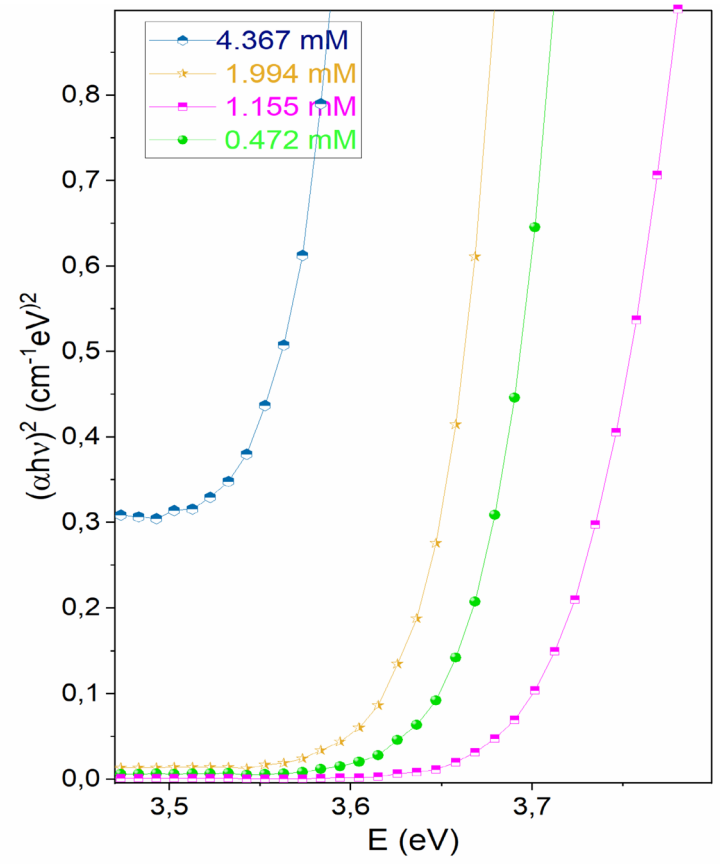

Fig. 6 Plot of $(\alpha h\upsilon)^2$ versus E at 4.367, 1.994, 1.155 and 0.472 mM concentrations of Pt(II) metal complex

applied to the p-Si's bright surface to form an active layer film, which was left to dry. Finally, Ag metal was evaporated onto the Pt(II) metal complex active layer, completing the diode preparation.

Current–voltage measurements of the diode were conducted using a KEITHLEY 2400 Current–Voltage Source at room temperature under dark conditions and different illumination intensities (50 and 100 mW/cm^2). Figure 7 displays the current–voltage (I-V) characteristics of the Pt(II) complex-based diode under these conditions. The graph demonstrates that the diode's current–voltage characteristics vary significantly with different illumination intensities. The illumination intensity notably affects the photoconductivity of the Pt(II) complex-based diode, with higher light intensity resulting in increased photoconductivity.

Conclusion

This study presents a novel Schiff base (SB) along with its Pd(II) and Pt(II) metal complexes, ([$SBMCl_2$]•H_2O), where SB represents (E)−6-tert-butyl 3-ethyl 2-(3-methoxy-4-phenoxybenzylideneamino)−4,5-dihydrothieno[2,3-*c*]pyridine-3,6(7H)-dicarboxylate, M = Pd(II)and Pt(II)). These compounds were synthesized

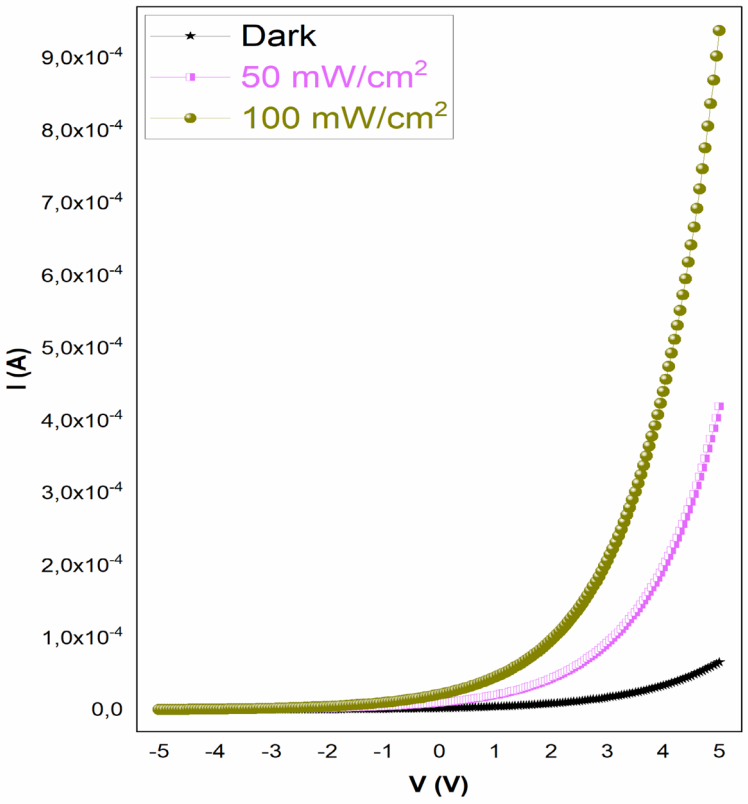

Fig. 7 Current–voltage (I-V) characteristics of Pt(II) complex-based diode under dark, 50 and 100 mW/cm^2 illumination conditions

for the first time and extensively characterized using various analytical techniques, including elemental analysis, NMR spectroscopy, FT-IR, electronic spectra, mass spectrometry, powder XRD, molar conductivity, magnetic susceptibility, and thermal analysis. The proposed structures for these compounds were determined based on analytical data and supporting literature. The study subsequently investigated the electronic and photonic properties of the thiophene-pyridine-based SB and its Pd(II) and Pt(II) complexes under varying conditions, determining their corresponding parameters. Furthermore, the researchers fabricated metal complex-based diodes and investigated their electronic and photonic characteristics. I-V measurements revealed that the palladium complex-based diode exhibited significant noise and high leakage current. In contrast, the Pt(II) complex-based diode demonstrated increased photoconductivity with rising light intensity.

The researchers conclude that the Schiff base ligand and its Pd(II) and Pt(II) complexes show promise for use in electronic and photonic devices. However, they acknowledge that further development would be necessary to achieve high-efficiency applications in these fields.

Supplementary Information The online version contains supplementary material available at https://doi.org/10.1007/s11164-025-05547-y.

Acknowledgements The authors extended their appreciation to the Researchers Supporting Muş Alparslan University BAP Project number BAP-21-FEF-4901-02.

Author contributions N.T. involved in project administration, resources, formal analysis, investigation, methodology, data curation, supervision, validation, writing-original draft, writing-review & editing. K.B. involved in investigation, methodology, validation, supervision, writing original draft. H.S. took part in formal analysis, investigation, methodology, data curation, validation. B.G involved in investigation, methodology, data curation, validation, writing original draft. N.Ç. took part in formal analysis, investigation, methodology, data curation, validation.

Funding Open access funding provided by the Scientific and Technological Research Council of Türkiye (TÜBİTAK).

Data availability No datasets were generated or analysed during the current study.

Declarations

Conflict of interest The authors declare no competing interests.

References

1. M.A. Ayoub, J. Mol. Struct. **1173**, 17 (2018)
2. S.H. Sumrra, M. Anees, A. Asif, M.N. Zafar, K. Mahmood, M.F. Nazar, M. Khalid, M.A. Nadeem, M.U. Khan, Bull. Chem. Soc. Ethiop. **34**(2), 335 (2020)
3. C.E. Satheesh, P.R. Kumar, P. Sharma, K. Lingaraju, B.S. Palakshamurthy, H.R. Naika, Inorganica Chim. Acta **442**, 1 (2016)
4. N. Turan, K. Buldurun, E. Bursal, G. Mahmoudi, J. Organomet. Chem. **970–971**, 122370 (2022)
5. N. Turan, K. Buldurun, N. Çolak, İ Özdemir, Open Chem. **17**(1), 571 (2019)
6. A.A. Abdel Aziz, R.G. Mohamed, F.M. Elantabli, S.M. El-Medani, J. Fluoresce. **26**(6), 1927 (2016)
7. R.G. Mohamed, F.M. Elantabli, A.A. Abdel Aziz, H. Moustafa, S.M. El-Medani, J. Mol. Struct. **1176**, 501 (2019)
8. A. Altun, J. Lumin. **271**, 120593 (2024)
9. W. Sawodny, M. Riederer, Angew. Chem. Int. Ed. Engl. **16**, 859 (1977)
10. N. Turan, H. Körkoca, R. Adigüzel, N. Çolak, K. Buldurun, Molecules **20**(5), 9309 (2015)
11. N. Turan, A. Savcı, K. Buldurun, Y. Alan, N. Çolak, Lett. Org. Chem. **13**(5), 343 (2016)
12. M.E. Alkış, K. Buldurun, N. Turan, Y. Alan, Ü. Keleştemur Yılmaz, A. Mantarcı, J. Biomol. Struct. Dyn. **40**(9), 4073 (2022)
13. A. Savcı, N. Turan, K. Buldurun, M.E. Alkış, Y. Alan, Inorg. Chem. Commun. **143**, 109780 (2022)
14. R.M. Ramadan, L.H. Abdel-Rahman, M. Ismael, T.A. Youssef, S.A. Ali, J. Mol. Struct. **1049**, 7 (2013)
15. N. Turan, A. Akdeniz, Catal. Lett. **153**(10), 3009 (2023)
16. K. Buldurun, N. Demir, N. Turan, M. Bingöl, J. Coord. Chem. **77**(12–14), 1541 (2024)
17. H. Seymen, N. Berk, İ Orak, Ş Karataş, J. Mater. Sci. Mater. Electron. **33**(24), 19656 (2022)
18. A. Türüt, Turk. J. Phys. **44**(4), 302 (2021)
19. S.M. Sze, Y. Li, K.K. Ng, *Physics of semiconductor devices*, 4th edn. (John Wiley & Sons, Hoboken, 2021)
20. F.Z. Bayat, H. Doğan, M. Şeker, J. Eng. Fac. **2**(1), 16 (2024)
21. N. Turan, H. Seymen, B. Gündüz, K. Buldurun, N. Çolak, Opt. Mater. **148**, 114802 (2024)
22. N. Turan, K. Buldurun, B. Gündüz, N. Çolak, J. Electron. Mater.ectron. Mater. **12**, 1028 (2017)
23. N. Turan, J. Electron. Mater. **48**, 7366 (2019)
24. N. Çolak, A. Karayel, K. Buldurun, N. Turan, J. Struct. Chem. **62**(1), 37 (2021)
25. Y. Dong, Y. Wang, Y. Song, Z. Yu, Z. Yu, Z. Zhao, L. Wang, ChemistrySelect **9**, e202400389 (2024)
26. Z. Jia, J. Cao, W. Chen, Z. Yu, Y. Song, Y. Dong, J. Fluoresc. **3**, 245 (2024)
27. I.A. Gencer, R.H.B. Syan, M. Gülcan, Y.S. Ocak, A. Tombak, J. Mater. Sci. Mater. Electron. **29**(2), 898 (2018)
28. M. Gaber, H.A. El-Ghamry, S.K. Fathalla, Spectrochim. Acta A Mol. Biomol. Spectrosc. **139**, 396 (2015)
29. P. Jayaseelan, E. Akila, M. Usha Rani, R. Rajavel, J. Saudi Chem. Soc. **20**(6), 625 (2016)
30. G. Ayyannan, M. Mohanraj, G. Raja, N. Bhuvanesh, R. Nandhakumar, C. Jayabalakrishnan, Inorg. Chim. Acta **453**, 562 (2016)
31. M. Gülcan, M. Sönmez, I. Berber, Turk. J. Chem. **36**, 189 (2012)
32. M. Elsherbeny, U. El-Ayaan, Y.G.A. El-Reash, G.M.A. El-Reash, Appl. Organomet. Chem. **39**, e7822 (2024)
33. S.A. Al-Aghbari, O.M. Al-Shuja, R. Al-Badani, M. Al-Wali, A. Japir, J. Mater. Sci. Chem. Eng. **7**, 1 (2019)
34. S. Jahangiry, M. Lashanizadegan, P.S. Pourhosseini, M. Zahedi-Tabrizi, Biometals **37**, 1161 (2024)
35. N. Gligorjevic, T. Todorovic, S. Radulovic, D. Sladic, N. Filipovic, D. Godevac, D. Jeremic, K. Andelkovic, Eur. J. Med. Chem. **44**, 1623 (2009)
36. R. Naskar, P. Ghosh, C.K. Manna, N. Murmu, T.K. Mondal, Inorganica Chim. Acta **534**, 120802 (2022)
37. H.F. Abd El-Halim, G.G. Mohamed, M.N. Anwar, Appl. Organomet. Chem. **32**, e3899 (2018)
38. K. Buldurun, N. Turan, A. Altun, N. Çolak, İ Özdemir, J. Mol. Struct. **1309**, 138185 (2024)

Authors and Affiliations

Nevin Turan[1] · Kenan Buldurun[2] · Halil Seymen[3] · Bayram Gündüz[4] · Naki Çolak[5]

✉ Nevin Turan
n.turan@alparslan.edu.tr

Kenan Buldurun
k.buldurun@alparslan.edu.tr

Halil Seymen
h.seymen@alparslan.edu.tr

Bayram Gündüz
Bayram.gunduz@ozal.edu.tr

Naki Çolak
nakicolak@hitit.edu.tr

[1] Department of Chemistry, Faculty of Arts and Sciences, Muş Alparslan University, 49250 Muş, Türkiye

[2] Department of Medical Services and Techniques, Health Services Vocational School, Muş Alparslan University, 49250 Muş, Türkiye

[3] Technical Sciences Vocational High School, Muş Alparslan University, 49250 Muş, Türkiye

[4] Department of Engineering Basic Sciences, Faculty of Engineering and Natural Sciences, Malatya Turgut Özal University, 44000 Malatya, Türkiye

[5] Department of Chemistry, Faculty of Arts and Sciences, Hitit University, 19100 Çorum, Türkiye